# On the Safety of Multiple Satellite Formations for Synthetic Aperture Radar Applications

Francesca Scala *, Maxwell Nogueira Peixoto†, Gerhard Krieger‡ and Michelangelo Villano§
*German Aerospace Center (DLR), Oberpfaffenhofen, 82234 Wessling, Germany*

## Nomenclature

| | | |
|---|---|---|
| $a_c$, $a_j$ | = | semi-major axis, m |
| $b_\perp$ | = | orthogonal baseline between a couple of satellites, m |
| $C_D$ | = | dimensionless drag coefficient, - |
| $e_{x_c}$, $e_{y_c}$, $e_{x_j}$, $e_{y_j}$ | = | $x$ and $y$ components of the eccentricity vector, - |
| $i_c$, $i_j$ | = | orbital inclination, rad |
| $j$ (or $k$) | = | subscript for the deputy satellites $j = 1, ..., N-1$ (or $k$) |
| $M$ | = | spacecraft mass, kg |
| $N$ | = | number of satellites, - |
| $S$ | = | spacecraft cross-sectional area, $m^2$ |
| $u_c, u_j$ | = | mean argument of latitude, rad |
| $\boldsymbol{\alpha}_c$, $\boldsymbol{\alpha}_j$ | = | non-singular Keplerian elements $\{a, u, e_x, e_y, i, \Omega\}$, $\{m, rad, -, -, rad, rad\}$ |
| $\delta\boldsymbol{\alpha}_j$ | = | quasi-non-singular relative orbital elements for deputy j |
| $\delta\boldsymbol{\alpha}_{jk}$ | = | extended relative orbital elements for the $\{j, k\}$ couple of deputies |
| $\delta e_j$, $\varphi_j$ | = | magnitude and phase of the relative eccentricity vector for deputy $j$, $\{-, rad\}$ |
| $\delta i_j$, $\theta_j$ | = | magnitude and phase of the relative inclination vector for deputy $j$, $\{-, rad\}$ |
| $\delta r_{x,z_{min}}$ | = | minimum relative distance in the radial and across-track direction, m |
| $\Delta B$ | = | difference of ballistic coefficient $B$ between a deputy and the chief, $m^2/kg$ |
| $\Omega_c$, $\Omega_j$ | = | right ascension of the ascending node, rad |
| $\|\| \cdot \|\|$ | = | $l_2$ norm of a vector |
| $(\cdot)_c$, $(\cdot)_j$ | = | chief and deputies subscript |

*Post-Doctoral Researcher, Microwaves and Radar Institute, francesca.scala@dlr.de (Corresponding Author)
†Doctoral Student, Microwaves and Radar Institute, maxwell.nogueirapeixoto@dlr.de
‡Head of Department Radar Concepts, Microwaves and Radar Institute, Gerhard.Krieger@dlr.de
§Head of the NewSpace SAR Group, Microwaves and Radar Institute, Michelangelo.Villano@dlr.de

# I. Introduction

The concept of multiple spacecraft flying in formation has become a key technology in space exploration over the last decade. Several studies demonstrated that it could improve mission reliability with coordinated platforms and enhance the science return [1–4]. In the context of Earth observation in low Earth orbit (LEO), numerous applications would incredibly benefit from tight formations of multiple spacecraft. Notably, formation flying played a crucial role in the success of the TanDEM-X (TerraSAR-X add-on for Digital Elevation Measurement) mission [4], making significant advancements in the field of synthetic aperture radar (SAR) interferometry. The deployment of two spacecraft in close proximity within a helix formation has proven crucial in mitigating the temporal decorrelation inherent in repeat-pass interferometry, enabling single-pass observations. The concept of the helix formation, in combination with the relative eccentricity/inclination vector separation concept, was introduced to ensure the passive safety of operations and establish effective baselines for SAR interferometry [5, 6]. Consequently, the TanDEM-X mission could benefit from larger baselines compared to a boom, as in the Shuttle Radar Topography Mission [7]. Larger baselines guarantee a smaller standard deviation of the height accuracy for the same standard deviation of the interferometric phase. As a result, TanDEM-X allowed generating a global digital elevation model (DEM) with unprecedented height accuracy and spatial resolution [4]. However, having only two spacecraft flying in formation limits the potentiality of future SAR applications. Already within the TanDEM-X mission, multiple acquisitions with different baselines were needed to cope with phase unwrapping errors [8].

This paper deals with distributed systems of three or more satellites, opening a multitude of applications to enhance future SAR missions. In this context, we have identified some primary applications that would benefit from a swarm of three or more satellites. The first concept, within the single-pass multibaseline interferometry, was proposed in [9], where a principal satellite and a primary deputy were considered in combination with one or more CubeSat add-on, flying in a nested helix orbit configuration. This approach enables the detection and resolution of phase unwrapping errors without compromising the final DEM, taking advantage of interferometric measurements with multiple baselines in a single pass. A similar concept is based on distributed interferometric SAR, denoted as MirrorSAR [10]. This configuration consists of one transmitting and multiple receiving spacecraft. The mission proposal High-Resolution Wide-Swath (HRWS) exploits this concept, considering a system of three receiving satellites [11], but one could also consider the case of a larger number of receiving satellites with multiple along-track and across-track baselines [12]. A similar application is multistatic tomography, where numerous platforms are strategically distributed in the across-track directions, serving either transmit-receive or transmit-only functions, depending on the operational mode [13–15]. Finally, the concept of multiple-input-multiple-output SAR consists of multiple transmitters and receivers to generate a large number of baselines with a minimal number of antennas [16, 17], and allows for the discrimination of different scattering mechanism in tomography [16].

The correct geometry set-up of a multi-platform system is crucial for generating multiple baselines in a single pass.

Additionally, an almost constant baseline ratio, among small and large baselines, is desirable for phase unwrapping purposes [18]. These requirements influence the design of the relative motion and should be coupled with a rigorous safety analysis to avoid any collision risk or unsafe behavior. Specifically, the safety of satellites flying in close proximity is a crucial aspect of the mission analysis itself [19–21].

A strategy to minimize the collision hazard for such formations was proposed in [6], where the concept of eccentricity/inclination (e/i) vector separation in geostationary orbits was adopted and extended to LEO applications. This approach immediately assesses the collision risk based on the formation set up in relative orbital elements (ROE). It is based on the minimum radial and across-track separation in time of a couple of spacecraft when high uncertainties are present in the along-track direction. This strategy was successfully applied to the TanDEM-X mission, demonstrating the potentiality of the technique. Subsequently, it was included in several mission concepts, such as the PRISMA (Hyperspectral Precursor and Application Mission) experiment [22], the VISOR ( VIrtual Super Optics Reconfigurable Swarm) mission concept [23], and on-orbit servicing mission studies [24]. Different from these studies, which consider a formation of two spacecraft, the work in [25] presents guidance and control techniques for a swarm of multiple spacecraft, aiming at maximizing their number in a given space volume. In addition, the work extended the concept of relative e/i vector separation to the case of a swarm of satellites. Similarly, other authors included the collision avoidance and safety considerations as a constraint in the model predictive control algorithm of spacecraft relative motion, as in [26, 27], or in the convex formulation of the optimal maneuver planning, as in [28, 29]. These works represent safety as a convex keep-out zone to compute feasible maneuver solutions.

Building upon the latest advancement, this work proposes a procedure to assess the safety of a space system involving multiple spacecraft. In contrast to the work in [25], the analysis in this paper incorporates the requirements and limitations imposed by a multi-platform SAR system for a preliminary mission design. The key outcomes of [9, 10] are adopted for SAR applications, and the concept of nested helix orbits serves as the baseline for the formation configuration. Additionally, the effect of the main external LEO perturbations, for example, atmospheric drag and Earth's oblateness, is included to represent the relative dynamics accurately. The inclusion of differential drag becomes crucial when there is a significant difference in the mass properties of different satellites, as between CubeSats and medium-class satellites. Modeling and incorporating the Earth's oblateness is essential for an accurate simulation of satellites in LEO. It has the effect of modifying the passive safety of the parallel e/i vector: it generates a drift in the relative eccentricity vector, leading towards an orthogonal condition.

This work envisions two main contributions to the state of the art within this context. First, it demonstrates that the passive safety of bounded relative motion can be designed, including SAR interferometry requirements. The condition on the large and small baseline ratio from [9] is formulated as a constraint in the ROE space, limiting the acceptable range of initial conditions for the formation set-up. Moreover, the mass and cross-sectional area difference is included as a constraint on spacecraft's ballistic coefficients. Second, it adopts and extends the safety approach in [6, 25] for multiple

satellites in a formation, including considerations for spacecraft with different orbit inclinations and initial phases of the relative motion. From these premises, Sec. II examines the requirements for a multibaseline SAR interferometric system, and describes the methodology adopted for the design of a safe formation, including the guidance and control architecture. Then, Sec. III presents simulated mission scenarios to validate the methodology and demonstrate the accomplishment of the passive safety for distributed SAR systems, whereas Sec. IV draws the conclusions and outcomes.

## II. Methodology

This section outlines the methodology employed for computing the safety condition of a space system consisting of a primary satellite (the chief) and a generic number, denoted as $N-1$, of secondary spacecraft (the deputies). Given the principal objective of this paper, namely, the development of a procedure for assessing the safety of a distributed system for SAR application, the workflow begins by identifying the requirements for single-pass multibaseline interferometry and their formulation in terms of the ROE framework. As illustrated in Fig. 1, the subsequent step consists of executing a routine to evaluate the safety of different geometries, with the goal being the selection of initial conditions that adhere to both SAR and safety constraints. The relative motion is described in terms of ROE, which serve three primary purposes: 1) providing a relative state description of the deputies around the chief satellite; 2) incorporating the mean Earth's oblateness, $J_2$ and the differential drag perturbations into the relative motion for accurate trajectory propagation; and 3) computing the safety condition of the deputies around the chief satellite. The inclusion of external orbital

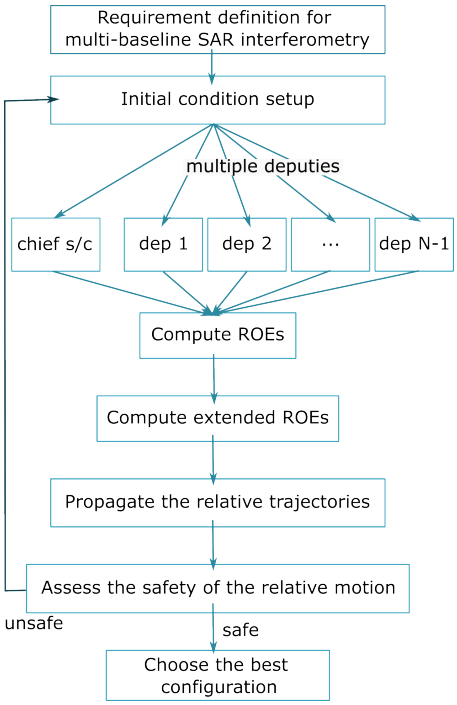


**Fig. 1 Workflow of the routine for safety assessment of different formation configurations.**

perturbations serves for the assessment of the safety condition in a more realistic orbital environment, which includes the effect of different physical properties among the platforms. In this analysis, the absolute Keplerian orbits of the chief and the deputies are assumed to be quasi-circular, with an equal semi-major axis to ensure a bounded relative motion. Differently from previous works, such as [6, 25], no assumptions are made upon the other orbital elements of the deputies. Specifically, the orbit inclinations of the deputies are not constrained to a common plane during the derivation. Additionally, a novel procedure is introduced to compute: 1) an analytical expression to assess the relative orbital elements of each couple of deputy satellites in terms of chief's absolute elements and deputies' ROE only; and 2) the extension of the safety condition to each pair of deputies.

### A. SAR Interferometry Requirements

This work investigates multi-platform space systems for single-pass across-track SAR interferometry based on the architecture proposed in [9]. As aforementioned, a space mission with a network of SAR instruments has the advantage of simultaneously acquiring two or more images from different positions [18]. The geometry plays a crucial role in the DEM performance: an example is shown in Fig. 2 [9]. The separation among the spacecraft, i.e., the baseline, affects the achievable spatial resolution and height estimation accuracy. The concept in [9] identifies the requirements when large and small baselines are involved, analyzing their ratio. Specifically, the ratio between the large and the small orthogonal baselines shall ideally be in the order of 2.5 to 4 to guarantee accurate interferograms. The orthogonal baseline, called $b_{\perp}$, is the component of the baseline perpendicular to the line of sight. The requirement for the baseline ratio influences the relative orbit design procedure and the control algorithms, which should consider the risk of potential collisions among the satellites in the formation. These aspects are investigated in the following.

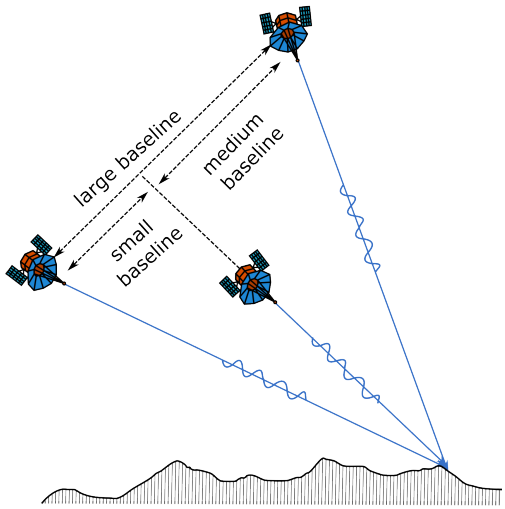


**Fig. 2 Multi-platform SAR system with large, small, and medium baselines.**

### B. Relative Orbital Elements Framework

The procedure adopted in this paper is based on the representation of the absolute orbits with non-singular Keplerian elements for quasi-circular orbits, as in [30, 31]. The orbit of the chief satellite is described by $\boldsymbol{\alpha}_c = \{a_c, u_c, e_{x_c}, e_{y_c}, i_c, \Omega_c\}$, where $a_c$ is the semi-major axis, $u_c = \omega_c + M_c$ is the mean argument of latitude, which depends on the argument of perigee $\omega_c$ and the mean anomaly $M_c$, $i_c$ is the orbit inclination, and $\Omega_c$ is the orbit right ascension of the ascending node. The x and y components of the eccentricity vector are defined by the eccentricity and argument of perigee of the chief: $e_{x_c} = e_c \cos\omega_c$ and $e_{y_c} = e_c \sin\omega_c$, respectively, where $e_c$ is the orbit eccentricity. Similarly, the orbit of the $j$-th deputy, with $j = 1, ..., N-1$, can be defined as $\boldsymbol{\alpha}_j = \{a_j, u_j, e_{x_j}, e_{y_j}, i_j, \Omega_j\}$. Consequently, the relative motion of the $j$-th deputy around the chief is described by the quasi-non-singular ROE, in polar notation [30]:

$$\delta\boldsymbol{\alpha}_j = \begin{Bmatrix} \delta a_j \\ \delta\lambda_j \\ \delta e_{x_j} \\ \delta e_{y_j} \\ \delta i_{x_j} \\ \delta i_{y_j} \end{Bmatrix} = \begin{Bmatrix} (a_j - a_c)/a_c \\ u_j - u_c + (\Omega_j - \Omega_c)\cos i_c \\ e_{x_j} - e_{x_c} \\ e_{y_j} - e_{y_c} \\ i_j - i_c \\ (\Omega_j - \Omega_c)\sin i_c \end{Bmatrix} = \begin{Bmatrix} (a_j - a_c)/a_c \\ u_j - u_c + (\Omega_j - \Omega_c)\cos i_c \\ \delta e_j \cos\varphi_j \\ \delta e_j \sin\varphi_j \\ \delta i_j \cos\theta_j \\ \delta i_j \sin\theta_j \end{Bmatrix}, \tag{1}$$

where the term $\delta\lambda_j$ is the mean argument of latitude, the terms $\delta e_j$ and $\varphi_j$ are the magnitude and phase of the relative eccentricity vector $\delta\boldsymbol{e}_j = \{\delta e_{x_j},\ \delta e_{y_j}\}$, whereas $\delta i_j$ and $\theta_j$ are the magnitude and phase of the relative inclination vector $\delta\boldsymbol{i}_j = \{\delta i_{x_j},\ \delta i_{y_j}\}$. This work assumes equal semi-major axes between the chief and the deputies, resulting in $\delta a_j = 0$ for every $j = 1, .., N-1$. Note that for each $j$-th satellite, the phases of the relative vectors $\delta\boldsymbol{e}_j$ and $\delta\boldsymbol{i}_j$ might differ.

### C. Extended Relative Orbital Elements

Following the definition of the ROE framework, an additional representation of the relative motion between deputy $j$ and deputy $k$ (with $j \neq k$) becomes of primary importance for the scope of this study. Accordingly, we introduce a supplementary notation to characterize the relative trajectory of deputy $j$ in relation to deputy $k$: the extended relative orbital elements (eROE). This representation relies solely on deputies' ROE and chief's orbital elements. The purpose of this notation is to extend the relative dynamics evolution to encompass an arbitrary deputy couple $\{j, k\}$: at each instant, the eROE provide information on the relative state among each deputy pair, giving an additional insight on the safety of the swam of spacecraft. The computation of eROE involves the combination of Eq. 1 and the Keplerian

representation of the absolute orbits $\boldsymbol{\alpha}_c$ for the generic pair $\{j,k\}$:

$$\delta\boldsymbol{\alpha}_{jk} = \begin{Bmatrix} \delta a_{jk} \\ \delta\lambda_{jk} \\ \delta e_{x_{jk}} \\ \delta e_{y_{jk}} \\ \delta i_{x_{jk}} \\ \delta i_{y_{jk}} \end{Bmatrix} = \begin{Bmatrix} \delta a_k - \delta a_j \\ \delta\lambda_k - \delta\lambda_j + \frac{\delta i_k \sin\theta_k - \delta i_j \sin\theta_j}{\tan i_c}\left(\frac{\cos(\delta i_j \cos\theta_j + i_c)}{\cos i_c} - 1\right) \\ \delta e_k \cos\varphi_k - \delta e_j \cos\varphi_j \\ \delta e_k \sin\varphi_k - \delta e_j \sin\varphi_j \\ \delta i_k \cos\theta_k - \delta i_j \, sin\theta_j \\ \left(\delta i_k \sin\theta_k - \delta i_j \sin\theta_j\right) \frac{\sin(\delta i_j \cos\theta_j + i_c)}{\sin i_c} \end{Bmatrix}. \tag{2}$$

Note that the expression in Eq. 2 differs from the analysis in [25], as we drop the assumptions of equal orbital inclinations. This aspect could result in a higher control effort to keep the formation and should be included in the mission design procedure. In fact, only for the particular case of $i_j = i_k = i_c$, Eq. 2 simplifies to $\delta\boldsymbol{\alpha}_{jk} = \delta\alpha_k - \delta\alpha_j$. An example of a formation of one chief and five deputies is shown in Fig. 3, where on the left, the initial conditions in terms of relative eccentricity vector components are reported, whereas the graph on the right represents the corresponding eROE. The subscript $(\cdot)_{jk}$ represents the eROE for the deputies' couple $j$ and $k$.

### D. Analytical Perturbed Relative Dynamical Model

Following the definition of ROE and eROE framework, this paragraph presents the relative dynamics model used for the analyses, which is based on a first-order linear approximation of the dynamics, parameterized in terms of ROE. Differently from the classical Hill-Clohessy-Wiltshire equations, we use a model including the first-order approximation of the mean $J_2$ and differential drag effects, starting from the works in [6, 25]. The differential drag perturbation is

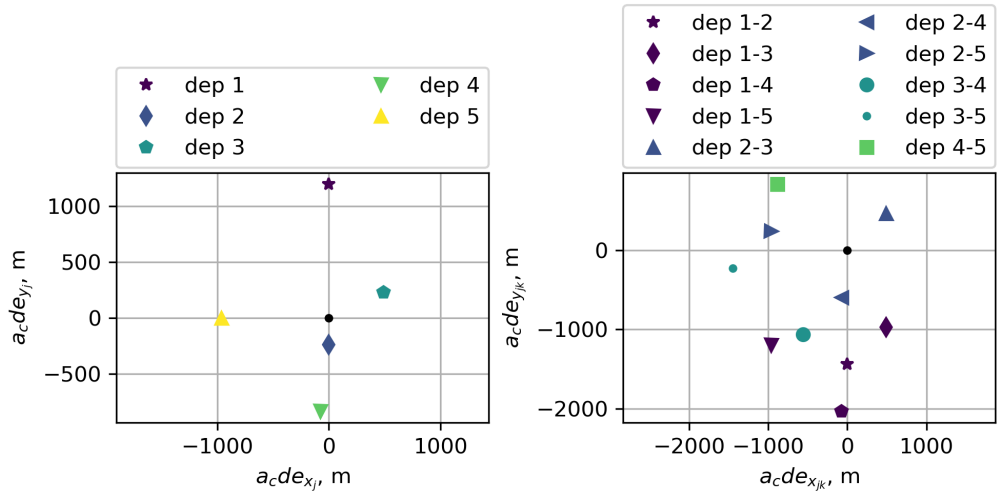


**Fig. 3 Example of initial conditions in ROE (left) and their mapping into eROE (right).**

included to model the effect of different physical properties (e.g., spacecraft mass or cross-sectional area) among the deputies. The relative trajectory is described using $\{x, y, z\}$ components, representing the relative position vector in a Cartesian Hill frame [32]. Figure 4 shows the local Hill frame for the formation of one chief and multiple deputies' spacecraft. The vectors $\mathbf{r}_1$, $\mathbf{r}_2$, ..., $\mathbf{r}_{N-1}$ represents the relative position of the deputy trajectories around the chief, where the $x$ axis is in the radial direction, the $z$ axis is in the direction of the angular momentum of chief's orbit (across-track), and the $y$ axis completes the right-hand side frame in the direction of motion (along-track). The dynamical equations for each $j$-th deputy is the following:

$$\begin{cases} x_j/a_c &= \delta a_j - \delta e_j \cos(u - \varphi_j - \dot{\varphi}_j \Delta u) - \frac{1}{n^2}\Delta B \rho v^2 \Delta u \\ y_j/a_c &= \delta\lambda_j - \frac{21}{2}\left(\gamma \sin(2i_c)\delta i_{x_j} + \frac{1}{7}\delta a_j\right)\Delta u + 2\delta e_j \sin(u - \varphi_j - \dot{\varphi}_j \Delta u) + \frac{3}{4n^2}\Delta B\, \rho v^2 \Delta u^2 \,, \\ z_j/a_c &= \delta i_{x_j}\left(\sin u - 3\sin^2\gamma \Delta u \cos u\right) - \delta i_{y_j}\cos u \end{cases} \tag{3}$$

where $\Delta u = u(t) - u(t=0)$ is the variation of the mean argument of latitude, with $u = nt$, where $n = \sqrt{\mu/a_c^3}$ is the mean motion of chief's orbit, with $\mu$ the gravitational constant, and $t$ is the time variable. The parameter $\gamma = \frac{J_2}{2}\left(\frac{R_p}{a_c}\right)^2 \frac{1}{\eta}$ describes the effect of the second-order zonal coefficient $J_2$, where $R_p$ is the central planet mean equatorial radius, and $\eta = \sqrt{1 - e_c^2}$. The variation of the phase of the relative eccentricity vector is $\dot{\varphi} = \frac{3}{2}\gamma\left(5\cos^2 i_c - 1\right)$, and the contribution of the differential drag is given by the differential ballistic coefficient $\Delta B = B_d - B_c$, where $B = C_D \frac{S}{M}$ is the ballistic coefficient, $C_D$ is the aerodynamic drag coefficient, $S$ is the spacecraft cross-sectional area, and $M$ is the spacecraft mass. The model in Eq. 3 has been validated in previous research [6], which demonstrated that, for an eccentricity and inclination vector separation with a magnitude between 200 m and 2000 m, the model can provide a solution with

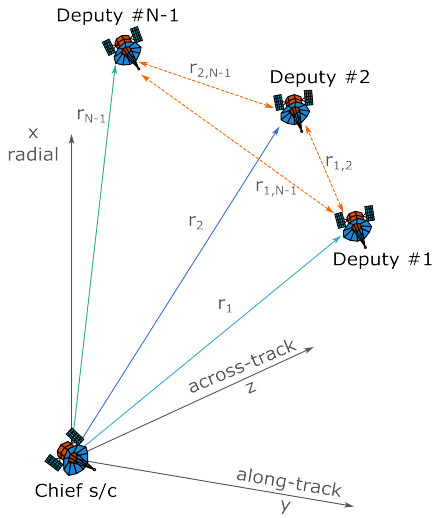


**Fig. 4 Local Hill frame for a generic formation of $j = 1, .., N-1$ deputies.**

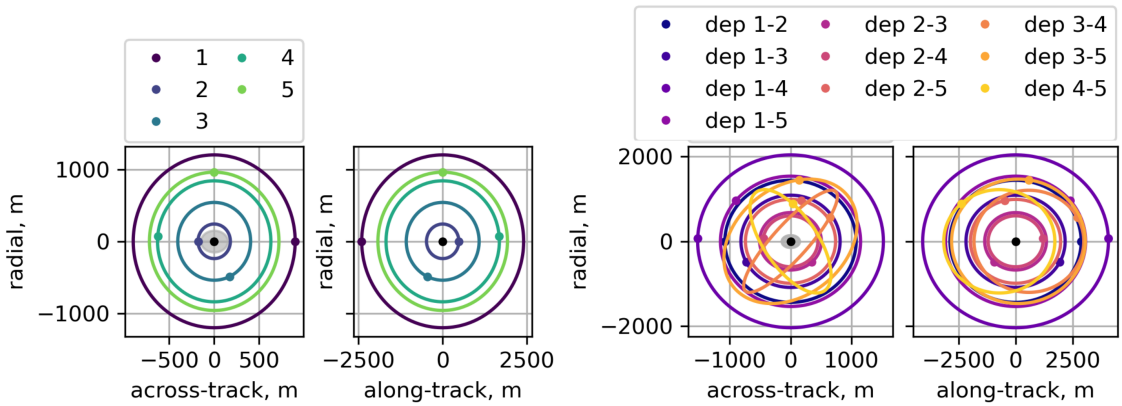


**Fig. 5 Example of a formation with $N = 6$. representations of ROE (left) and eROE (right).**

an accuracy in the order of a few meters. The formulation in Eq. 3 can be easily extended to represent the relative trajectory among a generic couple $\{j, k\}$ of deputies by substituting the ROE with the corresponding eROE in Eq. 2 for the corresponding couple. An example of trajectories for a formation with five deputies is shown in Fig. 5. The initial conditions of the deputies' trajectories are taken from Fig. 3, and they are propagated for one orbital period, assuming the same ballistic coefficient for the spacecraft (i.e. $B_j = B_k = B_c$). The trajectories on the left show the relative motion of the deputies around the chief, whereas the plot on the right describes the relative trajectory for the corresponding $\{j, k\}$ couple of deputies. Note that a central grey circle is shown in the radial and across-track separation to identify the keep-out zone for safety purposes (150 m for this case). The condition for the safety is discussed hereafter in Sec. II.F.

### E. Decentralised Guidance, Navigation, and Control Architecture

This paragraph describes the procedure for the guidance set-up, considering a sequence of on-board satellite operations. The procedure is adapted from the analytical analysis presented in [33] and, subsequently, tailored to the specific scenario under study. This work assumes that each spacecraft can execute navigation tasks and estimate its absolute and relative states in relation to the chief. The sequence of actions executed by each satellite is illustrated in Fig. 6. The chief reconstructs its absolute state $y_c^{eme}$ in the Earth mean equator and equinox (EME) reference frame of January 2000 (J2000), from external sensors (e.g., Global Positioning System (GPS) or Global Navigation Satellite System (GNSS)). Afterward, it performs the conversions to the true-of-date (ToD) reference system, yielding $y_c^{tod}$, required to compute the osculating $\alpha_c$ and mean $\bar{\alpha}_c$ orbital elements. The mean orbital elements are subsequently combined with the ROE of each $j$-th deputy, $\delta\alpha_j$, to determine the current state of the overall formation. Specifically, the information on $\delta\alpha_j$ is exchanged at each time between the deputies and the chief, which enables the chief to compute the safety condition and monitor the overall status of the formation. Similarly, each $j$-th deputy retrieves its absolute state from the external sensors and transforms it into mean orbital elements $\alpha_j$. Simultaneously, it receives real-time updates on the current state of the chief and the other deputies. Using these inputs, each deputy computes the safety condition

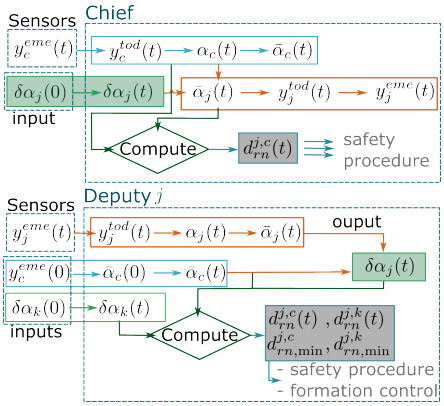


**Fig. 6 Guidance procedure for computing the safety condition of a multiple satellite formation flying.**

and, when necessary, initiates procedures to minimize the collision risk, such as maintenance or evasive maneuvers. In this paper, we make the hypothesis that only the deputies can perform corrective maneuvers to compensate for unsafe events, and set up the transition to a new safe configuration.

### F. Extension of the Relative e/i Vector Separation Concept

After defining the analytical model for relative dynamics, this section presents the derivation and extension of the relative e/i vector separation concept for safety analysis purposes. The condition for the safety procedure is computed in terms of the separation in the radial ($x$) and across-track ($z$) direction of the relative motion: $\delta r_{xz_j} \geq \delta r_{xz_{\min}}$, where the subscript $(\cdot)_{\min}$ is the minimum separation. This approach is based on the relative e/i separation proposed in [6, 34], in terms of magnitude and phase of the relative eccentricity and inclination vectors. Specifically, under the hypothesis of $\delta a = 0$, the relative eccentricity vector defines the separation in the radial direction, whereas the inclination vector defines the separation out-of-plane (i.e., in the across-track direction). In the absence of external perturbations, the minimum separation between two spacecraft can be expressed as [25]:

$$\|\delta\mathbf{e}_j \cdot \delta\mathbf{i}_j\| \geq \frac{\delta r_{xz_{\min}}}{a_c}\sqrt{\delta e_j^2 + \delta i_j^2 - \frac{\delta r_{xz_{\min}}^2}{a_c^2}} \tag{4}$$

This expression is valid for $j$-th deputy and poses a constraint on the magnitude and phase of the relative eccentricity vector. Under the assumption that the phase of the $\delta\mathbf{i}_j$ vector is $\theta = 90$ deg, we obtain the following expression:

$$\left(\delta e_j \sin\varphi_j\right)^2 \geq \left(\frac{a_c^2\delta i_j^2}{r_{xz_{\min}}^2} - 1\right)^{-1} \delta e_j^2 \cos^2\varphi_j + \frac{\delta r_{xz_{\min}}^2}{a_c^2} \tag{5}$$

This expression describes a hyperbolic exclusion zone in the ROE framework for each $j$-th deputy. Representing the relative motion among each couple of deputies via the eROE makes it possible to extend the safety condition to each

couple $\{j, k\}$. Specifically, writing Eq. 5 in terms of eROE, we get the following expression:

$$\left(\delta e_{jk} \sin \varphi_{jk}\right)^2 \geq \left(\frac{a_c^2 \delta i_{jk}^2}{r_{xz_{\min}}^2} - 1\right)^{-1} \delta e_{jk}^2 \cos^2 \varphi_{jk} + \frac{\delta r_{xz_{\min}}^2}{a_c^2}, \tag{6}$$

where the same minimum distance condition is considered as in Eq. 5. Equation 5 is a general expression valid for different initial phases of the relative eccentricity vectors of each deputy. In this work, Eqs. 5 and 6 are used to preliminary design a multiple satellite formation geometry.

## III. Results

This section illustrates the practical applications of the safety conditions outlined in Sec. II.F. The analysis focuses on two specific case scenarios: 1) a parametric analysis is conducted to select the initial conditions for a formation of three SAR satellites; and 2) an analytical analysis is performed to identify the exclusion zone in ROE space, taking into account the SAR and the safety perspectives. In both analyses, we make the assumption that $\delta a_j = 0$ and $\delta \lambda_j = 0$, with $j = 1, ..., N-1$. The methodology for these scenarios relies on the possibility of expressing the ROE of the generic $k$-th deputy (with $k \neq j$) as a function of the ROE of deputy $j$ ($\delta \boldsymbol{\alpha}_j$), incorporating two multiplicative factors denoted as $k_{e_k}$ and $k_{i_k}$. These factors are used to quantify the magnitude of the relative eccentricity and inclination vectors of the $k$-th deputy, expressed as $\delta e_k = k_{e_k} \delta e_j$, and $\delta i_k = k_{i_k} \delta i_j$, respectively.

### A. Parametric Analysis

The first analysis focuses on a formation of three SAR satellites. Specifically, it aims to assess the possibility of adding a third satellite (denoted as "add-on") between the chief and the primary deputy (denoted as "deputy no.1") to achieve both a large and a small baseline in a single pass for an accurate and robust DEM acquisition. Table 1 details the initial conditions for the parametric analysis. We assume a look angle of 36.4 deg for interferometry [9], and we incorporate both the mean $J_2$ and the differential drag contributions in the orbit propagation. Furthermore, we assume the deputy no.1 to have similar ballistic properties with the chief, differing by only 1%. In contrast, the add-on satellite has a 20% difference in ballistic coefficient to account for different mass and cross-section properties of the third satellite, as in the case of a CubeSat. For the analysis, we compute $50 \times 50$ combinations of the magnitude of $\delta e$ and $\delta i$ for the deputy no.1, whereas, regarding the add-on spacecraft, we consider two combinations of multiplicative factors $(k_e,\ k_i)$ and three combinations of phase angles $(\varphi,\ \theta)$. The values for $k_e,\ k_i$ were chosen as upper and lower limit conditions to satisfy the ratio between large and small baselines, as explained in Sec. II.A. To assess the safety condition (as per Eq. 4), we propagate the relative trajectories for one day under external perturbations, considering a minimum distance threshold of $\delta r_{x,z_{min}} = 150$ m, from the safety condition of TanDEM-X [4]. The results of this parametric analysis are presented as maps, illustrating feasible conditions for the magnitude of the relative eccentricity and inclination

**Table 1 Initial conditions for the parametric analysis**

| Parameters | Value |
|---|---|
| *Chief satellite* | |
| Altitude, km | 400 |
| Eccentricity, - | 0.0001 |
| Inclination, deg | 98.3 |
| Ballistic coefficient, - | 0.006 |
| *Deputy satellite no.1* | |
| Ballistic coefficient, - | 0.00606 |
| Relative eccentricity $a\delta e$, m | [150 : 1000] |
| Relative inclination $a\delta i$, m | [150 : 1000] |
| Phase angle $\varphi$, deg | 90 |
| Phase angle $\theta$, deg | 270 |
| *Add-on satellite* | |
| Ballistic coefficient, - | 0.0072 |
| Multiplicative factor $k_e$, - | $[0.25, 0.4]$ |
| Multiplicative factor $k_i$, - | $[0.25, 0.4]$ |
| Phase angle $\varphi$, deg | $[45, 90, 135]$ |
| Phase angle $\theta$, deg | $[225, 270, 315]$ |

vectors, considering different phase angles. Each map of feasible conditions describes the solution for the range of $\delta e$ and $\delta i$ for deputy no.1 and is produced for each $k_e$, $k_i$ value and for each set of phase angles. Consequently, each map represents the feasible conditions in terms of safety and DEM requirements for the selection of initial conditions of a formation made by a chief, a deputy, and an add-on. Figures 7, 8, 9, and 10 showcase these results. Figure 7 illustrates the map of feasible conditions considering $k_e = k_i = 0.25$ and the set of phase angles of $\theta = 270$ deg and $\varphi = [45,\ 90,\ 135]$ deg, for the add-on deputy. The map shows that a feasible set of $\delta e$ and $\delta i$ for deputy no.1 is achieved only for the combination of $\theta = 270$ deg and $\varphi = 90$ deg, whereas for the other cases, there is no feasible solution. As expected, the former condition corresponds to parallel eccentricity and inclination vectors of the add-on, in phase with the relative trajectory of deputy no.1. Figure 8 further demonstrates this result by considering different sets of parallel conditions of eccentricity and inclination vectors for the add-on deputy. A slightly more relaxed condition is obtained considering the multiplicative factors $k_e = k_i = 0.4$, as shown in Fig. 9. In this case, a range of feasible $\delta e$ and $\delta i$ can be obtained even when the add-on deputy has a different phase from the deputy no.1. Similarly, considering parallel eccentricity-inclination vectors and different phases produces a map of widely feasible solutions in terms of $\delta e$ and $\delta i$. Consequently, this parametric analysis illustrates that different initial conditions can be selected for the add-on spacecraft, respecting both the SAR large and small baseline ratio and the safety conditions. The feasible solutions include relative trajectories with the same phase of deputy no.1 (i.e., $\varphi = 90$ deg and $\theta = 270$ deg) and different phase values for the add-on satellites, resulting in a flexible range of initial conditions.

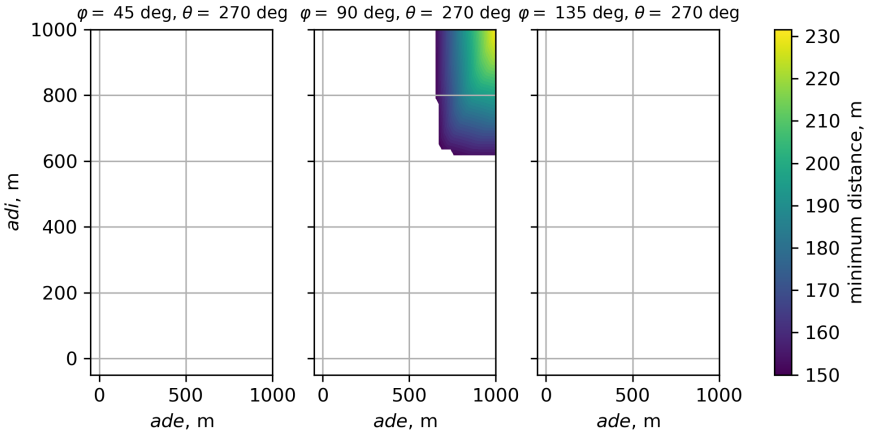


**Fig. 7 Parametric analysis for $k_e = k_i = 0.25$.**

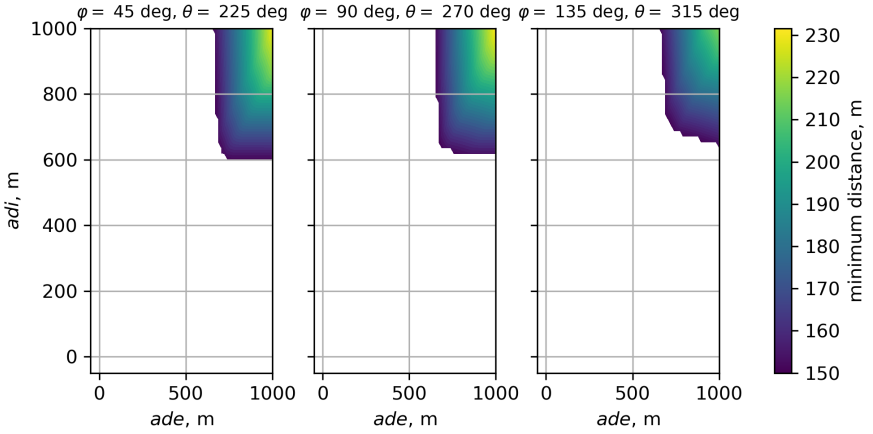


**Fig. 8 Parametric analysis for $k_e = k_i = 0.25$ and anti-parallel $\delta e/\delta i$.**

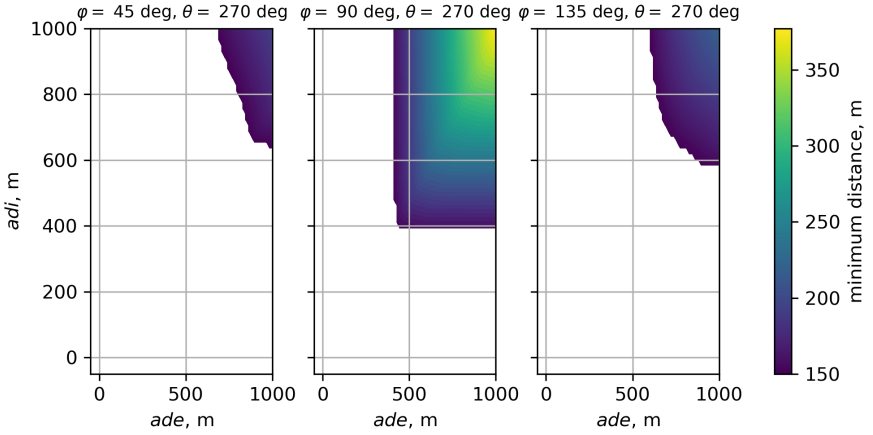


**Fig. 9 Parametric analysis for $k_e = k_i = 0.4$.**

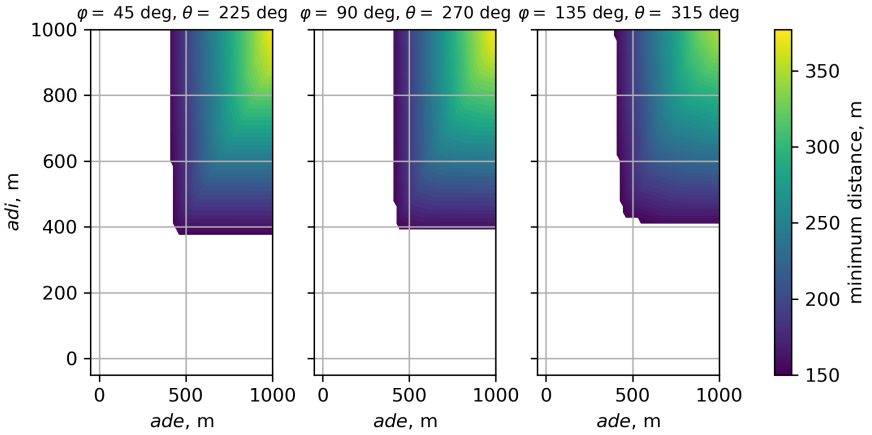


**Fig. 10 Parametric analysis for $k_e = k_i = 0.4$ and anti-parallel $\delta e/\delta i$.**

### B. Analytical solution for equal phase angles

The second analysis introduces an analytical approach to identify the range of initial conditions for the specific scenario of equal orbit inclinations among the satellites (i.e. $\theta_j = \theta_k = 90$ deg). In this case, we consider a configuration of multiple relative helix orbits in a nested arrangement [10], with spacecraft in phase: the phase angles are assumed equal among the deputies (i.e., $\varphi_k = \varphi_j = \varphi$). Under these conditions, two relations are derived from Eq. 6, describing the safety of the trajectory of $k$-the deputy with respect to the chief and the $j$-th deputy:

$$\left(\delta e_j \sin\varphi\right)^2 \geq \left(\frac{k_{i_k}^2}{k_{e_k}^2}\frac{a_c^2\delta i_j^2}{r_{xz_{\min}}^2} - 1\right)^{-1} k_{e_k}^2 \delta e_j^2 \cos^2\varphi + \frac{\delta r_{xz_{\min}}^2}{a_c^2}, \tag{7}$$

$$\left(\delta e_j \sin\varphi\right)^2 \geq \left(\frac{\left(k_{i_k}-1\right)^2}{\left(k_{e_k}-1\right)^2}\frac{a_c^2\delta i_j^2}{r_{xz_{\min}}^2} - 1\right)^{-1} \left(k_{e_k}-1\right)^2 \delta e_j^2 \cos^2\varphi + \frac{\delta r_{xz_{\min}}^2}{a_c^2}, \tag{8}$$

where Eq. 7 represents the safety condition for the $k$-th deputy with respect to the chief satellite, whereas Eq. 8 represents the combined safety for the satellite $k$ with respect to satellite $j$, ensuring mutual safety among the deputies.

To address distributed SAR missions, the conditions in Eqs. 6, 7, and 8 must be coupled with the specific application requirements. Specifically, maintaining the baseline ratio in the range 2.5 to 4 (see Fig. 2) introduces an additional constraint in the ROE framework, in terms of feasible multiplicative factors (i.e., $k_e$ and $k_i$). The exclusion zone for safety and SAR interferometry conditions is depicted in Fig. 11. The shaded light blue area represents the exclusion zone based on the constraint of the large and small baseline ratio (see Fig. 2). Conversely, the shaded grey hyperbolic area represents the exclusion zone for safety purposes. Each hyperbola is generated by a different value of the multiplicative factor $k_e$. Notably, as $k_e$ reduces, the safety constraint becomes more stringent in terms of feasible $\theta$ angles for the deputies, and vice versa. Considering the four add-on deputies of Fig. 11, we computed the corresponding orthogonal baseline and the corresponding ratio. Figure 12 shows the orthogonal baseline on top: the baseline of the deputy no.1

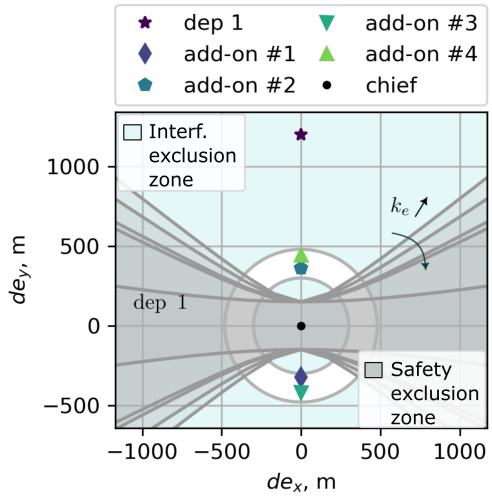


**Fig. 11 Exclusion zones for safety condition and SAR interferometry constraints.**

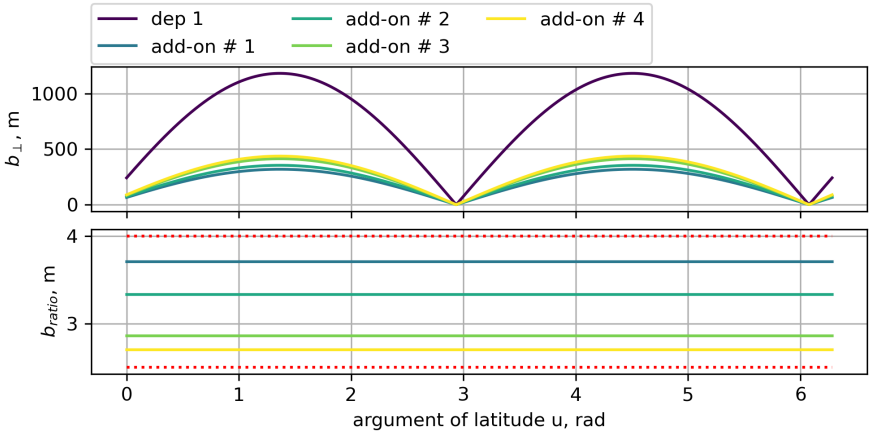


**Fig. 12 Baseline and baseline ratios for a SAR interferometry formation.**

and each add-on satellite is computed with the chief. It represents one large orthogonal baseline generated by the deputy no.1 and multiple small orthogonal baselines generated by the add-on satellites. Then, the baseline ratio is shown on the bottom plot of Fig. 12. The latter quantity is defined as:

$$b_{ratio} = \frac{b_{\perp_1}}{b_{\perp^i}}, \tag{9}$$

where the notation $b_{\perp_1}$ indicates the orthogonal baseline of deputy 1 with the chief satellite, whereas $b_{\perp^i}$ represents the orthogonal baselines of the add-on deputy $i$ (with $i = 1, .., 4$) with the chief satellite. Thus, the quantity $b_{ratio}$ represents the constraint described in Fig. 2, and it is limited by the dotted red lines, which represents the constraint imposed by the multi-platform space systems for single-pass across-track SAR interferometry (2.5 to 4). Consequently, this analysis defines a map with a safety area for the selection of the initial conditions of the add-on spacecraft, that

adhere to SAR interferometry requirements, as demonstrated in Fig.12. Note that the exclusion zone restricts both the magnitude $\delta e$ and the phase angle $\varphi$ of the eccentricity vector for the add-on spacecraft.

### C. Operational Considerations

To assess the feasibility of implementing the proposed approaches on a satellites, we evaluated the computational complexity of the methods. As expected, the parametric analysis is characterized by greater time and memory demands, resulting in a time and space complexity of $O(n^2 \times t)$ and $O(n^2)$, respectively. The parameter $n = 50$ denotes the number of combinations of magnitudes of the relative eccentricity and inclination vectors, and $t$ represents the number of time steps for the simulation. Substantially increasing the number of combinations and the time discretization has a significant impact on the performance of the method. In the simulations outlined in Section III.A, the execution time was 1.5 minutes, with a memory usage of about 20 KB on a laptop with a 1.9 GHz processor and 32 GB of RAM. Conversely, the analytical approach proves to be more efficient, requiring only 4 seconds of execution time and 4 KB of memory usage. For both methods, the estimated resource requirements for an off-the-shelf on-board computer are minimal, considering the current processing power available, typically in the range of a few hundred MHz to a few GHz, and the RAM capacity ranging from a few hundred MB to a few GB. For both the parametric and analytical methods, the estimated memory usage on board is below 10% and 2%, respectively, even for low-performance processors. For the case under analysis, the execution time does not represent a limitation for the proposed method.

Due to the nature of the helix relative trajectory, the safe initial conditions determined by the parametric or the analytical analysis starts to be affected by the external orbital perturbations over a span of several days. For example, in the case of TanDEM-X with (anti-)parallel relative $\delta\boldsymbol{e}$ and $\delta\boldsymbol{i}$, an unsafe condition is reached gradually over a period of approximately 20 to 30 days [30]. Consequently, TanDEM-X executes a control maneuver scheme twice per day to keep the safety of the formation and maintain the relative motion in the designated control tube. A similar consideration holds for the proposed methodologies, which aim to establish safety conditions robust against multiple days of uncontrolled propagation and communication failures among the satellites. Depending on the specific configuration, initial relative distance, and operational parameters, it is essential to assess the maximum acceptable duration in which the spacecraft can continue its nominal trajectory without safety adjustments. However, in order to hold a robust strategy for safety assessment, the proposed approaches should be implemented once or twice per day, to identify and plan corrective maneuvers for the subsequent day. It is noteworthy that in the long time period, if one deputy do not compensate for the effect of the external perturbations, the relative $\delta\boldsymbol{e}_j$ vector starts to drift toward a perpendicular condition with the relative $\delta\boldsymbol{i}_j$ vector, potentially leading to an unsafe scenario. These consideration should be studied in the eventuality one of these methodologies is adopted for mission design.

## IV. Conclusions

This manuscript establishes a methodology for computing the safety conditions to initialize a distributed mission tailored for multistatic SAR applications, particularly for single-pass multibaseline interferometry. The methodology addresses safety considerations when incorporating one or more additional spacecraft into a two-satellite formation. The introduction of the eROE in Sec. II enables the treatment of relative trajectories among a different couple of deputies as additional satellites in the formation, thereby facilitating their inclusion in the safety analysis. The first case scenario includes the impact of external orbital perturbations, including the differential drag for the case of significantly different ballistic coefficients (approximately 20% difference). Multiple maps are provided, considering a parametric variation in the magnitude and phase of the relative eccentricity and inclination vectors for the add-on satellite. The solution is derived by including the constraints on the multiplicative factors imposed by SAR interferometry. In contrast, the second case scenario focuses on a specific case where the phase angles of the relative eccentricity and inclination vectors are equal throughout the formation. This approach offers an immediate representation, in the ROE space, of the combined safety and interferometry exclusion zone, limiting the feasible magnitude and phase angle for the relative eccentricity vector. One limitation of the presented approach is the assumption of no separation in the semi-major axis and the mean argument of latitude. The condition of $\delta a = 0$, ensuring a close trajectory for the deputy, may be subject to uncertainties during the formation establishment or control errors, potentially impacting formation's safety. Additionally, the condition on the mean argument of latitude $\delta\lambda$ could be leveraged to introduce along-track separation, potentially beneficial for different applications. Although introducing a separation in along-track will not affect the safety condition presented in Secs II and III, in the absence of relative orbit control, introducing $\delta\lambda \neq 0$ could prevent collision among the satellites when the relative eccentricity and inclination vectors become orthogonal, due to external gravitational perturbations ($J_2$). However, this approach is typically impractical, as the navigation accuracy is less reliable in the along-track direction than the radial and across-track components. Finally, the proposed methodology could be leveraged introducing a constraint on fuel conservation, as this could be beneficial to minimize the propellant consumption.

## V. Funding Sources

This work was partially funded by the European Union (ERC Starting Grant Distributed Radar Interferometry and Tomography Using Clusters of Smallsats (DRITUCS) 101076275). Views and opinions expressed are however those of the authors only and do not necessarily reflect those of the European Union or the European Research Council Executive Agency. Neither the European Union nor the granting authority can be held responsible for them.

## References


[1] Di Mauro, G., Lawn, M., and Bevilacqua, R., "Survey on Guidance Navigation and Control Requirements for Spacecraft Formation-Flying Missions," *Journal of Guidance, Control, and Dynamics*, Vol. 41, No. 3, 2018, pp. 581–602. https://doi.org/10.2514/1.G002868.

[2] Llorente, J., Agenjo, A., Carrascosa, C., de Negueruela, C., Mestreau-Garreau, A., Cropp, A., and Santovincenzo, A., "PROBA-3: Precise formation flying demonstration mission," *Acta Astronautica*, Vol. 82, No. 1, 2013, pp. 38–46. https://doi.org/10.1016/j.actaastro.2012.05.029.

[3] Palacios, L., Ceriotti, M., and Radice, G., "Close proximity formation flying via linear quadratic tracking controller and artificial potential function," *Advances in Space Research*, Vol. 56, No. 10, 2015, pp. 2167–2176. https://doi.org/10.1016/j.asr.2015.09.005.

[4] Krieger, G., Moreira, A., Fiedler, H., Hajnsek, I., Werner, M., Younis, M., and Zink, M., "TanDEM-X: A Satellite Formation for High-Resolution SAR Interferometry," *IEEE Transactions on Geoscience and Remote Sensing*, Vol. 45, No. 11, 2007, pp. 3317–3341. https://doi.org/10.1109/TGRS.2007.900693.

[5] Moreira, A., Krieger, G., and Mittermayer, J., "Satellite configuration for interferometric and/or tomographic imaging of the earth's surface using synthetic aperture radar," *European Patent Office (no. EP1273518B1)*, 2002. URL https://patents.google.com/patent/EP1273518B1.

[6] D'Amico, S., and Montenbruck, O., "Proximity Operations of Formation-Flying Spacecraft Using an Eccentricity/Inclination Vector Separation," *Journal of Guidance, Control, and Dynamics*, Vol. 29, No. 3, 2006, pp. 554–563. https://doi.org/10.2514/1.15114.

[7] Farr, T. G., Rosen, P. A., Caro, E., Crippen, R., Duren, R., Hensley, S., Kobrick, M., Paller, M., Rodriguez, E., Roth, L., Seal, D., Shaffer, S., Shimada, J., Umland, J., Werner, M., Oskin, M., Burbank, D., and Alsdorf, D., "The Shuttle Radar Topography Mission," *Reviews of Geophysics*, Vol. 45, No. 2, 2007. https://doi.org/10.1029/2005RG000183.

[8] Lachaise, M., Fritz, T., and Bamler, R., "The Dual-Baseline Phase Unwrapping Correction Framework for the TanDEM-X Mission Part 1: Theoretical Description and Algorithms," *IEEE Transactions on Geoscience and Remote Sensing*, Vol. 56, No. 2, 2018, pp. 780–798. https://doi.org/10.1109/TGRS.2017.2754923.

[9] Nogueira Peixoto, M., Krieger, G., Moreira, A., Waldschmidt, C., and Villano, M., "On the Exploitation of CubeSats for Highly Accurate and Robust Single-Pass SAR Interferometry," *IEEE Transactions on Geoscience and Remote Sensing*, Vol. 61, 2023, pp. 1–16. https://doi.org/10.1109/TGRS.2023.3316895.

[10] Mittermayer, J., Krieger, G., Bojarski, A., Zonno, M., Villano, M., Pinheiro, M., Bachmann, M., Buckreuss, S., and Moreira, A., "MirrorSAR: An HRWS Add-On for Single-Pass Multi-Baseline SAR Interferometry," *IEEE Transactions on Geoscience and Remote Sensing*, Vol. 60, 2022, pp. 1–18. https://doi.org/10.1109/TGRS.2021.3132384.

[11] Bartusch, M., Bruens, C., Nuncio Quiroz, A. E., and Stettner, S., "HRWS: The upcoming German X-Band Spaceborne SAR Mission," *EUSAR 2021; 13th European Conference on Synthetic Aperture Radar*, 2021, Mar 29 - Apr 1, Leipzig, Germany, pp. 1–4. URL https://ieeexplore.ieee.org/abstract/document/9472672.

[12] Peixoto, M. N., Villano, M., Krieger, G., Moreira, A., and Waldschmidt, C., "A Novel Technique to Generate Digital Elevation Models in a Single Pass Using a Cluster of Smallsats," *IGARSS 2023 - 2023 IEEE International Geoscience and Remote Sensing Symposium*, 2023, pp. 8331–8334. https://doi.org/10.1109/IGARSS52108.2023.10282527.

[13] Grasso, M., Renga, A., Fasano, G., Graziano, M., Grassi, M., and Moccia, A., "Design of an end-to-end demonstration mission of a Formation-Flying Synthetic Aperture Radar (FF-SAR) based on microsatellites," *Advances in Space Research*, Vol. 67, No. 11, 2021, pp. 3909–3923. https://doi.org/10.1016/j.asr.2020.05.051.

[14] Krieger, G., "MIMO-SAR: Opportunities and Pitfalls," *IEEE Transactions on Geoscience and Remote Sensing*, Vol. 52, No. 5, 2014, pp. 2628–2645. https://doi.org/10.1109/TGRS.2013.2263934.

[15] Seker, I., and Lavalle, M., "Tomographic Performance of Multi-Static Radar Formations: Theory and Simulations," *Remote Sensing*, Vol. 13, No. 4, 2021, p. 737. https://doi.org/10.3390/rs13040737.

[16] Krieger, G., Rommel, T., and Moreira, A., "MIMO-SAR Tomography," *Proceedings of EUSAR 2016: 11th European Conference on Synthetic Aperture Radar*, 2016, June 6-9, Hamburg, Germany, pp. 1–6. URL https://ieeexplore.ieee.org/abstract/document/7559253.

[17] Tebaldini, S., Flora, L., and Rocca, F., "A Mimo Multi-Static SAR Satellite Formation for High Resolution 3D Imaging at Longer Wavelengths," *2021 IEEE International Geoscience and Remote Sensing Symposium IGARSS*, 2021, pp. 1086–1089. https://doi.org/10.1109/IGARSS47720.2021.9554685.

[18] Krieger, G., and Moreira, A., "Multistatic SAR Satellite Formations: Potentials and Challenges," *IEEE Geoscience and Remote Sensing Symposium*, Vol. 4, IEEE, 2005, Jul 25-29, Seoul, South Korea, pp. 2680–2684. URL https://ieeexplore.ieee.org/abstract/document/1525618.

[19] Patera, R. P., "Satellite Collision Probability for Nonlinear Relative Motion," *Journal of Guidance, Control, and Dynamics*, Vol. 26, No. 5, 2003, pp. 728–733. https://doi.org/10.2514/2.5127.

[20] Lee, D., Sanyal, A. K., and Butcher, E. A., "Asymptotic Tracking Control for Spacecraft Formation Flying with Decentralized Collision Avoidance," *Journal of Guidance, Control, and Dynamics*, Vol. 38, No. 4, 2015, pp. 587–600. https://doi.org/10.2514/1.G000101.

[21] Basu, H., Pedari, Y., Almassalkhi, M., and Ossareh, H. R., "Computationally Efficient Collision-Free Trajectory Planning of Satellite Swarms Under Unmodeled Orbital Perturbations," *Journal of Guidance, Control, and Dynamics*, Vol. 46, No. 8, 2023, pp. 1548–1563. https://doi.org/10.2514/1.G007206.

[22] D'Amico, S., Ardaens, J.-S., and Larsson, R., "Spaceborne Autonomous Formation-Flying Experiment on the PRISMA Mission," *Journal of Guidance, Control, and Dynamics*, Vol. 35, No. 3, 2012, pp. 834–850. https://doi.org/10.2514/1.55638.

[23] Koenig, A. W., D'Amico, S., and Lightsey, E. G., "Formation Flying Orbit and Control Concept for Virtual Super Optics Reconfigurable Swarm Mission," *Journal of Guidance, Control, and Dynamics*, Vol. 46, No. 9, 2023, pp. 1657–1670. https://doi.org/10.2514/1.G007334.

[24] Sellmaier, F., Boge, T., Spurmann, J., Gully, S., Rupp, T., and Huber, F., "On-Orbit Servicing Missions: Challenges and Solutions for Spacecraft Operations," *American Institute of Aeronautics and Astronautics, Inc.*, 2010. URL https://elib.dlr.de/63555/.

[25] Koenig, A. W., and D'Amico, S., "Robust and Safe N-Spacecraft Swarming in Perturbed Near-Circular Orbits," *Journal of Guidance, Control, and Dynamics*, Vol. 41, No. 8, 2018, pp. 1643–1662. https://doi.org/10.2514/1.G003249.

[26] Sauter, L., and Palmer, P., "Analytic Model Predictive Controller for Collision-Free Relative Motion Reconfiguration," *Journal of Guidance, Control, and Dynamics*, Vol. 35, No. 4, 2012, pp. 1069–1079. https://doi.org/10.2514/1.56521.

[27] Zagaris, C., Park, H., Virgili-Llop, J., Zappulla, R., Romano, M., and Kolmanovsky, I., "Model Predictive Control of Spacecraft Relative Motion with Convexified Keep-Out-Zone Constraints," *Journal of Guidance, Control, and Dynamics*, Vol. 41, No. 9, 2018, pp. 2054–2062. https://doi.org/10.2514/1.G003549.

[28] Sarno, S., Guo, J., D'Errico, M., and Gill, E., "A guidance approach to satellite formation reconfiguration based on convex optimization and genetic algorithms," *Advances in Space Research*, Vol. 65, No. 8, 2020, pp. 2003–2017. https://doi.org/10.1016/j.asr.2020.01.033.

[29] Scala, F., Gaias, G., Colombo, C., and Martín-Neira, M., "Design of optimal low-thrust manoeuvres for remote sensing multi-satellite formation flying in low Earth orbit," *Advances in Space Research*, Vol. 68, No. 11, 2021, pp. 4359–4378. https://doi.org/10.1016/j.asr.2021.09.030.

[30] D'Amico, S., Montenbruck, O., Arbinger, C., and Fiedler, H., "Formation Flying Concept for Close Remote Sensing Satellites," *American Astronautical Society (AAS) / American Institute of Aeronautics and Astronautics (AIAA) Space Flight Mechanics Conference*, Advances in the Astronautical Sciences, Vol. 120, AAS, 2005, pp. 831–848. URL https://elib.dlr.de/11475/.

[31] Hintz, G. R., "Survey of Orbit Element Sets," *Journal of Guidance, Control, and Dynamics*, Vol. 31, No. 3, 2008, pp. 785–790. https://doi.org/10.2514/1.32237.

[32] Clohessy, W., and Wiltshire, R., "Terminal guidance system for satellite rendezvous," *Journal of the aerospace sciences*, Vol. 27, No. 9, 1960, pp. 653–658. https://doi.org/10.2514/8.8704.

[33] Gaias, G., Colombo, C., and Lara, M., "Analytical Framework for Precise Relative Motion in Low Earth Orbits," *Journal of Guidance, Control, and Dynamics*, Vol. 43, No. 5, 2020, pp. 915–927. https://doi.org/10.2514/1.G004716.

[34] Koenig, A., D'Amico, S., and Lightsey, E. G., "Formation Flying Orbit and Control Concept for the VISORS Mission," *AIAA Scitech 2021 Forum*, 2021. https://doi.org/10.2514/6.2021-0423.